Electronic Supplementary Material (ESI) for Journal of Materials Chemistry C.

Supporting Information

Filter-free Color Image Sensor Based on $CsPbBr_{3-3n}X_{3n}$ (X=Cl, I) Single Crystals

Peng Zhang, Yunqiu Hua, Xiang Li, Longzhen Zhang, Lin Liu, Rongzhen Li, and Guodong Zhang, Xutang Tao**

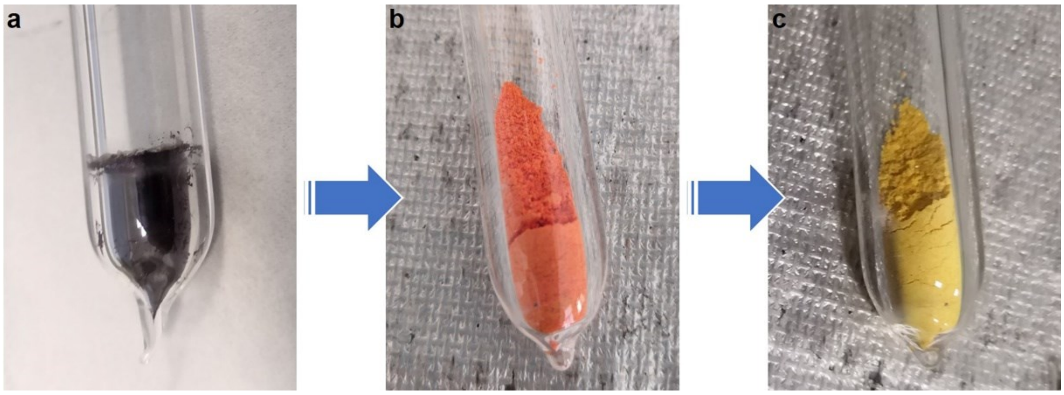

Fig. S1 (a) As-prepared $I_{1.5}$ polycrystal. (b) $I_{1.5}$ polycrystal after exposure to the room environment for 2 d. (c) $I_{1.5}$ polycrystal after exposure to the room environment for 5 d.

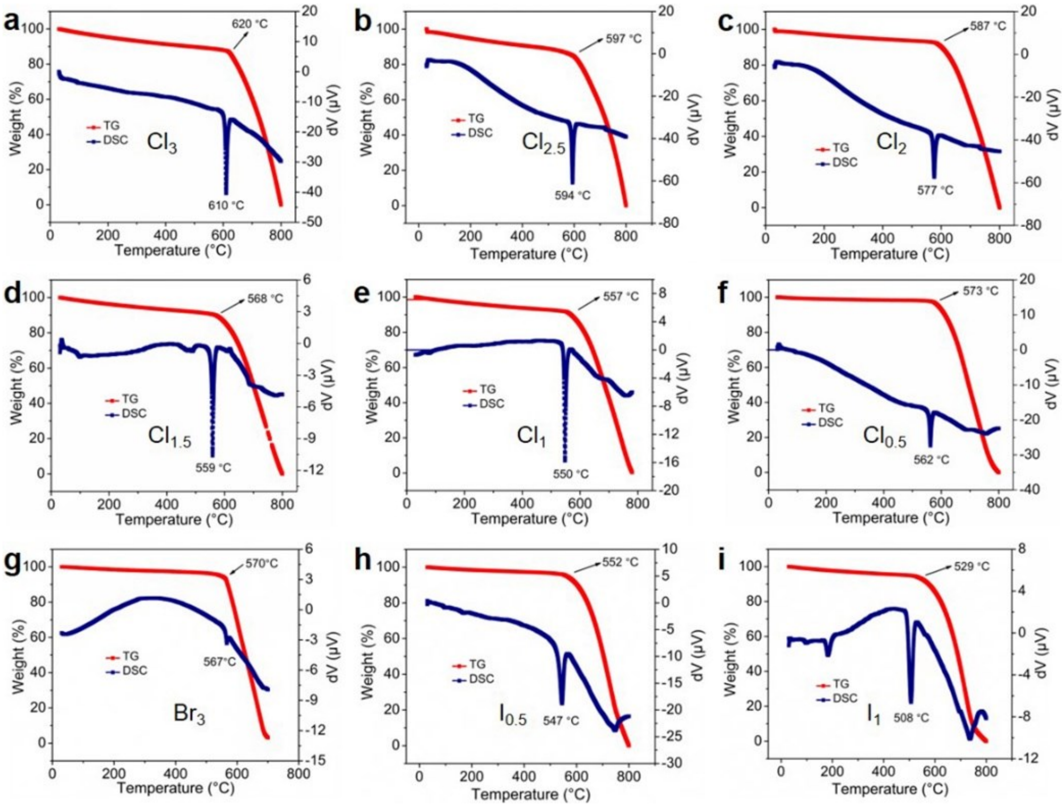

Fig. S2 Thermogravimetric-differential scanning calorimetry (TG-DSC) curves for the (a) Cl_3, (b) $Cl_{2.5}$, (c) Cl_2, (d) $Cl_{1.5}$, (e) Cl_1, (f) $Cl_{0.5}$, (g) Br_3, (h) $I_{0.5}$ and (i) I_1 crystals.

Fig. S2a-i show the TG-DSC curves for the Cl_3, $Cl_{2.5}$, Cl_2, $Cl_{1.5}$, Cl_1, $Cl_{0.5}$, Br_3, $I_{0.5}$, and I_1 crystals, respectively, obtained at melting points of 610, 594, 577, 559, 550, 562, 567, 547, and 508 °C, respectively.

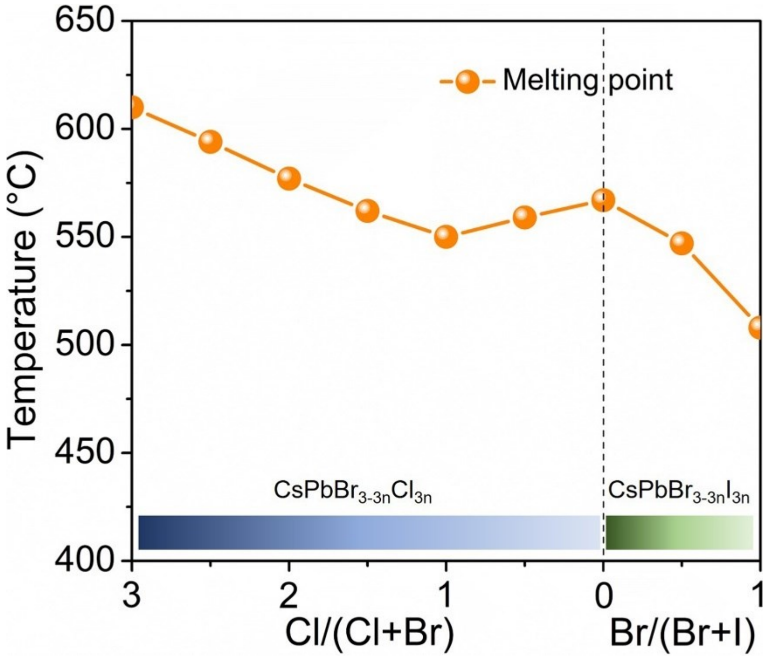

Fig. S3 Melting points of the $CsPbBr_{3-3n}X_{3n}$ crystals.

Fig. S3 shows the melting points depending on the compositions of $CsPbBr_{3-3n}X_{3n}$ crystals. The addition of I lowered the melting points of $CsPbBr_{3-3n}I_{3n}$ crystals. With the increase of I content, the melting point of $CsPbBr_{3-3n}I_{3n}$ crystal decreases. However, the situation of $CsPbBr_{3-3n}Cl_{3n}$ crystals is complicated. From Br_3 to Cl_1, the melting point of $CsPbBr_{3-3n}Cl_{3n}$ crystal decreases, while from Cl_1 to Cl_3, the melting point of $CsPbBr_{3-3n}Cl_{3n}$ crystal increases.

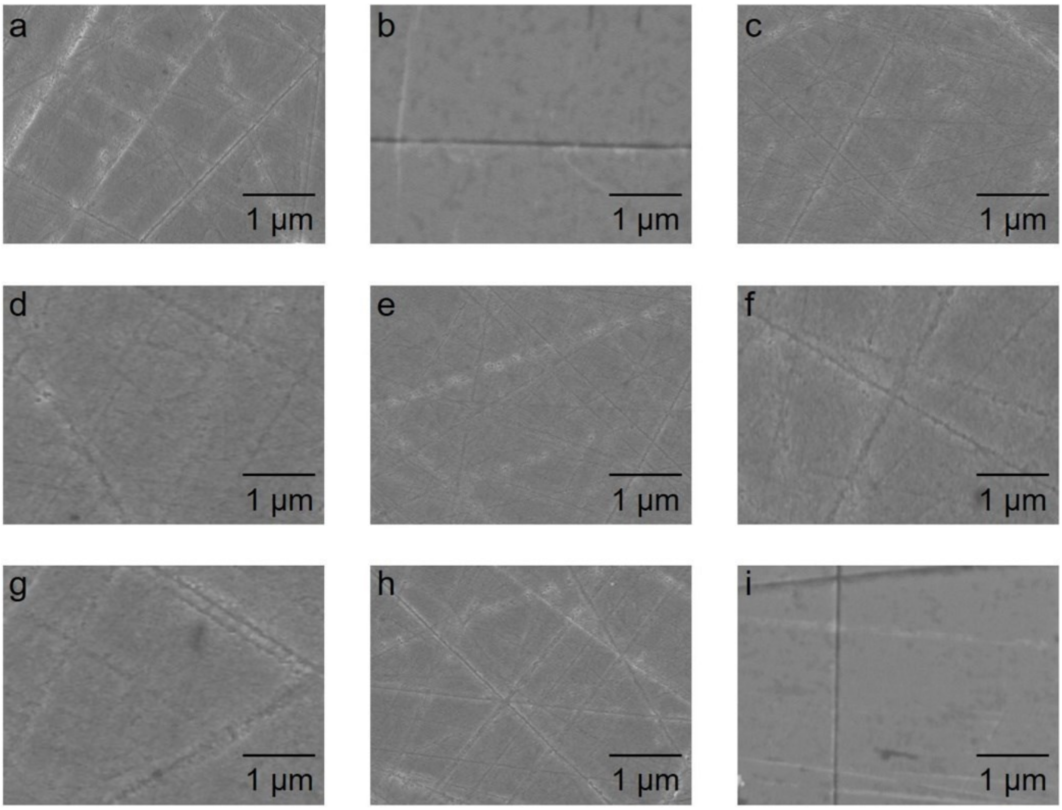

Fig. S4 Scanning electron microscope (SEM) of the polished (a) Cl_3, (b) $Cl_{2.5}$, (c) Cl_2, (d) $Cl_{1.5}$, (e) Cl_1, (f) $Cl_{0.5}$, (g) Br_3, (h) $I_{0.5}$ and (i) I_1 single crystal wafers.

Fig. S4a-i show the SEM of the Cl_3, $Cl_{2.5}$, Cl_2, $Cl_{1.5}$, Cl_1, $Cl_{0.5}$, Br_3, $I_{0.5}$ and I_1wafer, respectively. There are no defects such as grain boundaries or inclusions inside $CsPbBr_{3-3n}X_{3n}$ single crystals, which proves the high crystalline quality of these crystals. Defects on the crystal surface are scratches caused by processing.

Table S1 X-ray fluorescence (XRF) results of $CsPbBr_{3-3n}X_{3n}$ crystals.

	$Cl_{2.5}$	Cl_2	$Cl_{1.5}$	Cl_1	$Cl_{0.5}$	$I_{0.5}$	I_1
Br/mass%	7.02	16.7	23.9	15.3	37.0	31.5	27.5
Cl or I/mass%	21.4	15.0	11.0	15.6	2.96	14.2	19.3
Chemical formula	$CsPbBr_{0.44}Cl_{2.56}$	$CsPbBr_{0.99}Cl_{2.01}$	$CsPbBr_{1.53}Cl_{1.47}$	$CsPbBr_{2.06}Cl_{0.94}$	$CsPbBr_{2.54}Cl_{0.46}$	$CsPbBr_{2.46}I_{0.54}$	$CsPbBr_{2.08}I_{0.92}$

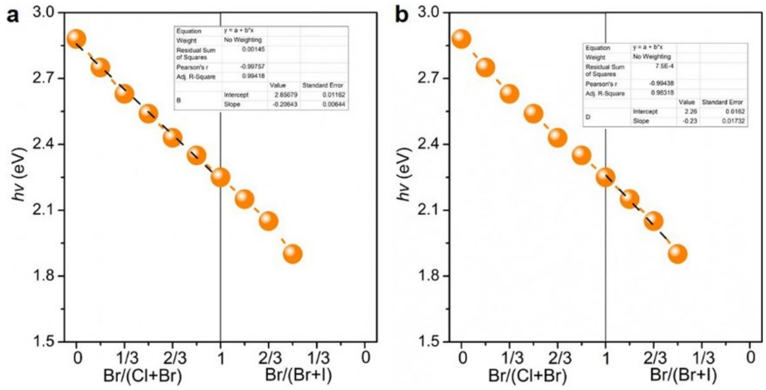

Fig. S5 Linear fitting of the optical band gap of the a) $CsPbBr_{3-3n}Cl_{3n}$ and b) $CsPbBr_{3-3n}I_{3n}$ crystals.

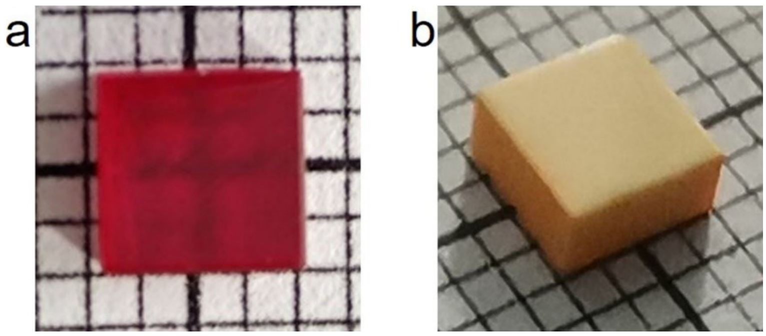

Fig. S6 Photographs of the (a) fresh cut I_1 crystal wafer and (b) the one put in the ambient atmosphere for a few hours.

Fig. S6a shows the fresh cut kermesinus I_1 crystal wafer. However, after a few hours, the kermesinus I_1 crystal putting in the ambient atmosphere changes to yellow as shown in Fig. S6b.

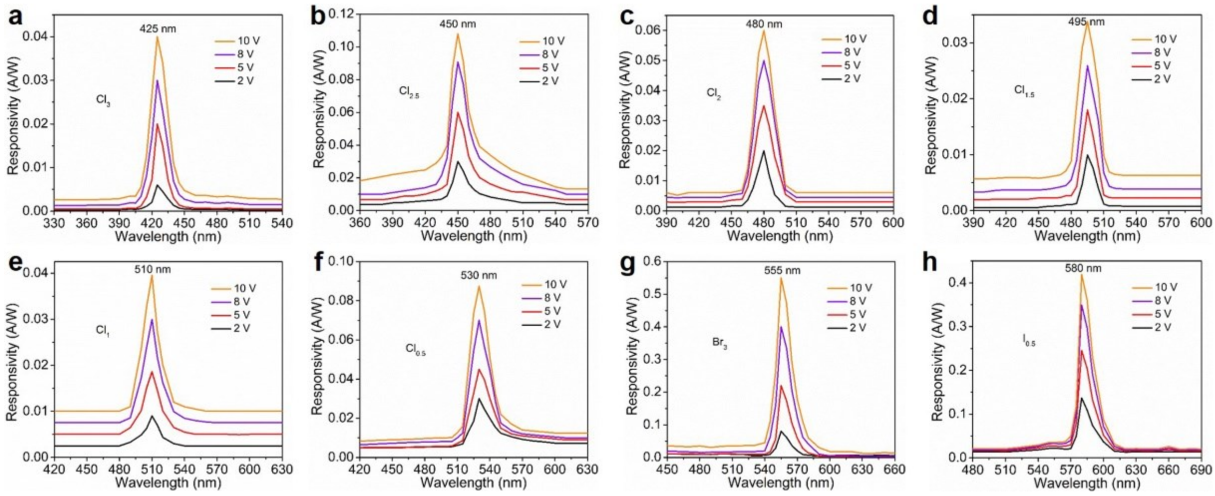

Fig. S7 Responsivity spectrum of the (a) Cl_3, (b) $Cl_{2.5}$, (c) Cl_2, (d) $Cl_{1.5}$, (e) Cl_1, (f) $Cl_{0.5}$, (g) Br_3, and (h) $I_{0.5}$ device at different bias voltages.

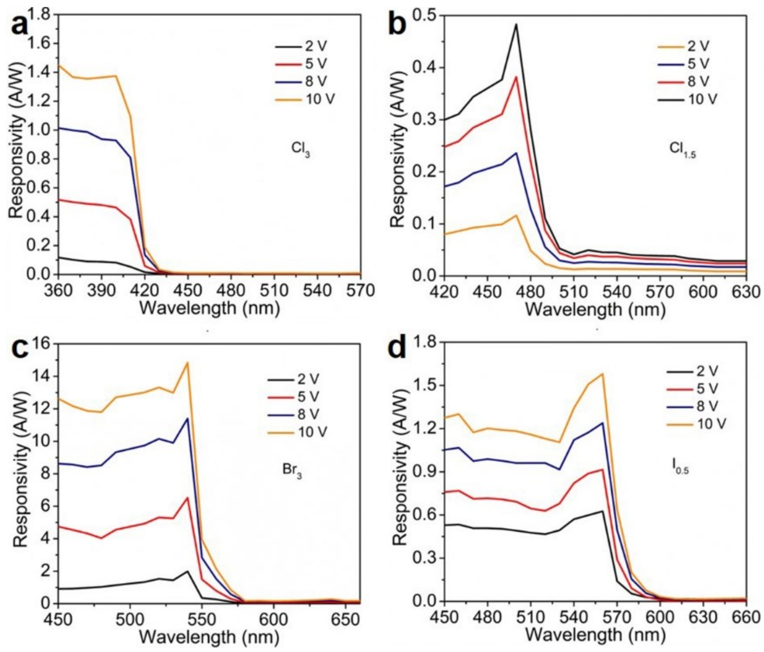

Fig. S8 Broadband photodetection spectrum of the (a) Cl_3, (b) $Cl_{1.5}$, (c) Br_3, and (d) $I_{0.5}$ device at different bias voltages.

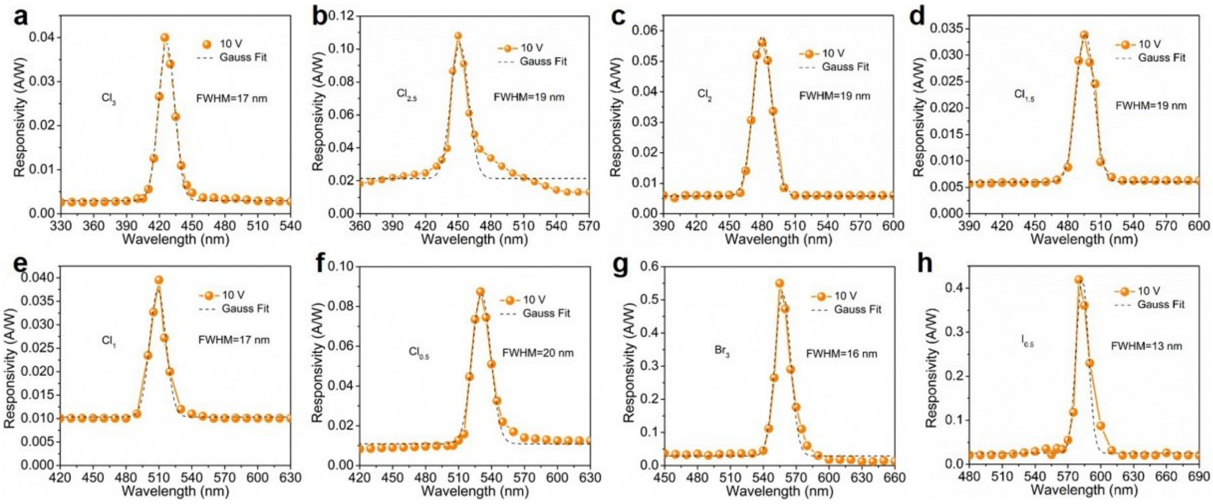

Fig. S9 FWHMs of the (a) Cl_3, (b) $Cl_{2.5}$, (c) Cl_2, (d) $Cl_{1.5}$, (e) Cl_1, (f) $Cl_{0.5}$, (g) Br_3, and (h) $I_{0.5}$ device at a bias voltage of 10 V.

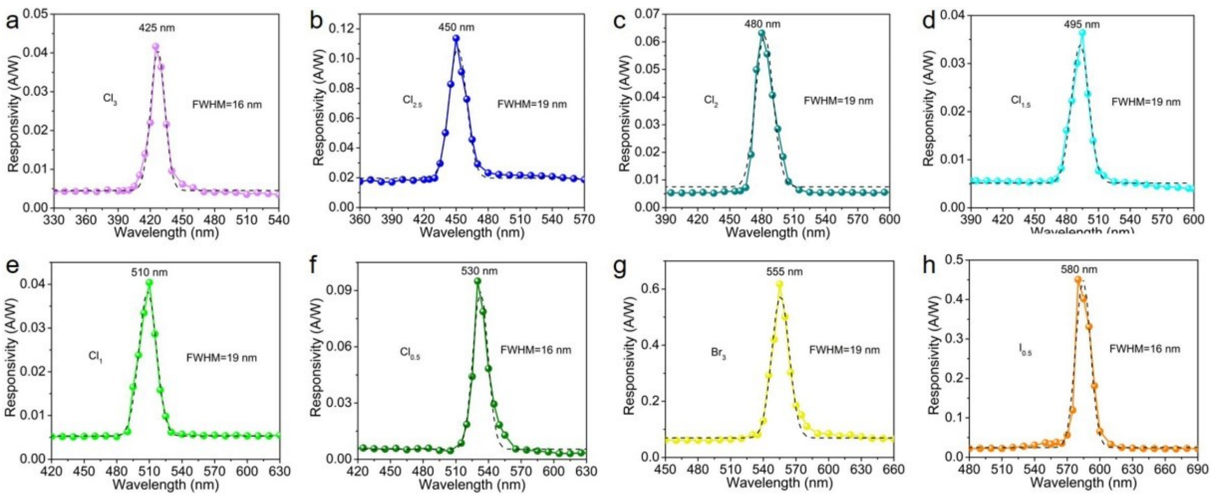

Fig. S10 Responsivity spectrum and FWHMs of the (a) Cl_3, (b) $Cl_{2.5}$, (c) Cl_2, (d) $Cl_{1.5}$, (e) Cl_1, (f) $Cl_{0.5}$, (g) Br_3, and (h) $I_{0.5}$ devices with 300 μm thickness at a bias voltage of 10 V.

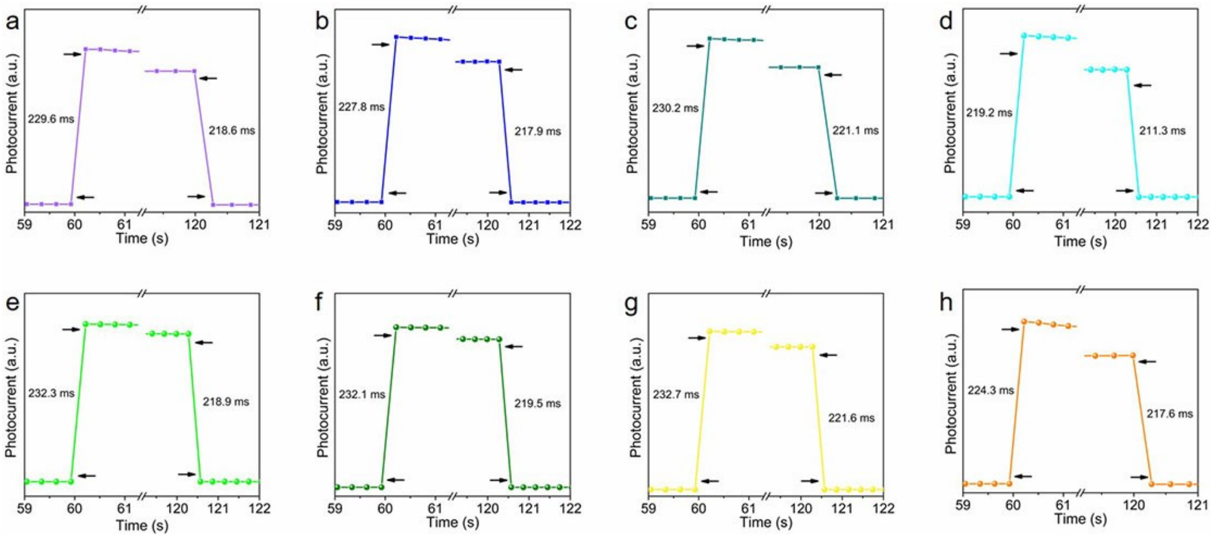

Fig. S11 I-t curves of the (a) Cl_3, (b) $Cl_{2.5}$, (c) Cl_2, (d) $Cl_{1.5}$, (e) Cl_1, (f) $Cl_{0.5}$, (g) Br_3, and (h) $I_{0.5}$ devices with 1.5 mm thickness at a bias voltage of 10 V.